Check for updates

FEBS openbio

FEBS PRESS science publishing by scientists

RESEARCH ARTICLE

Molecular characterization of *covRS* mutations in $M1_{UK}$ *Streptococcus pyogenes*

Jarrad Pritchard[1], Emma-Jayne Proctor[1], Jiawa Wang[1,2], Nikolas P. Johnston[1], Andrew Hayes[3], Georgia McCorkell[1], Haibo Yu[1,2], Jai Tree[4], Mark R. Davies[3], Mark J. Walker[5], Ronald Sluyter[1], Stephan Brouwer[5] and Martina L. Sanderson-Smith[1]

1 School of Science and Molecular Horizons, University of Wollongong, Australia
2 ARC Centre of Excellence in Quantum Biotechnology, University of Wollongong, Australia
3 The Peter Doherty Institute for Infection and Immunity, University of Melbourne, Australia
4 School of Biotechnology and Biomolecular Sciences, University of New South Wales, Sydney, Australia
5 Centre for Superbug Solutions, Institute for Molecular Bioscience, The University of Queensland, QLD, Australia

Keywords
covRS; $M1_{UK}$; phosphorylation-dependent dimerization; *Streptococcus pyogenes*; two-component regulatory system

Correspondence
Martina L. Sanderson-Smith, School of Science and Molecular Horizons, University of Wollongong, Northfields Aven, Wollongong, 2500, NSW, Australia
Tel: +61 2 42981935
E-mail: martina@uow.edu.au

Jarrad Pritchard, Emma-Jayne Proctor, Georgia McCorkell, Stephan Brouwer and Martina L. Sanderson-Smith contributed equally to this manuscript.

(Received 30 March 2026, revised 10 May 2026, accepted 15 May 2026)

doi:10.1002/2211-5463.70275

Increasingly invasive *Streptococcus pyogenes* disease has been linked to the emergence of the $M1_{UK}$ lineage. Here, we used a murine infection model to investigate the ability of $M1_{UK}$ to accumulate mutations in the *covRS* operon which regulates up to 15% of the genome, including multiple virulence factors. Assessing an $M1_{UK}$ isolate carrying an Ala111Val nonsynonymous mutation showed that *in vitro*, $M1_{UK}$ $CovR^{Ala111Val}$ was characterized by decreased SpeB expression, increased streptolysin O and hyaluronic acid capsule expression, and resistance to neutrophil killing. While Ala111Val represents a minor biochemical change, we show that $CovR^{Ala111Val}$ prevents phosphorylation-dependent dimerization. Specifically, molecular dynamics simulations suggest $CovR^{Ala111Val}$ destabilizes the interface between CovR monomers that facilitate dimerization, likely inhibiting CovR dimer-mediated transcriptional repression and promoting altered virulence factor expression. Ultimately, this work underscores the need for ongoing epidemiological surveillance to monitor the emergence of such mutations within the already hypervirulent $M1_{UK}$ lineage.

Streptococcus pyogenes (Group A *Streptococcus*; GAS) is a human-specific pathogen responsible for both superficial and invasive disease (iGAS). Superficial infections include self-limiting conditions such as impetigo and pharyngitis. However, when GAS disseminates through the epithelial and submucosal layers, it can result in iGAS diseases including necrotizing fasciitis, bacteraemia and streptococcal toxic shock syndrome (STSS) [1]. Recurrent GAS infection can also lead to autoimmune complications such as rheumatic heart disease (RHD). The global burden of GAS disease is estimated to exceed 500 000 deaths annually, of which approximately 160 000 are attributed to iGAS [2].

Over the past decade, an increase in the incidence of iGAS has been documented globally, at least partly

Abbreviations
GAS, Group A Streptococcus; iGAS, invasive Group A Streptococcus; LiKAP, lithium potassium acetyl phosphate; MD, molecular dynamics; RHD, rheumatic heart disease; RMSF, root-mean-square fluctuation; SLO, streptolysin O; SNPs, single nucleotide polymorphisms; SpeA, streptococcal pyrogenic exotoxin A; SpeB, streptococcal pyrogenic exotoxin B; SpeC, streptococcal pyrogenic exotoxin C; SSA, streptococcal superantigen; STSS, streptococcal toxic shock syndrome.

FEBS Open Bio (2026) © 2026 The Author(s). *FEBS Open Bio* published by John Wiley & Sons Ltd on behalf of Federation of European Biochemical Societies.
This is an open access article under the terms of the Creative Commons Attribution License, which permits use, distribution and reproduction in any medium, provided the original work is properly cited.

attributed to the emergence of the toxigenic $M1_{UK}$ lineage [3,4]. To date, cases of $M1_{UK}$ have been reported in Australia, Europe, Asia, as well as North and South America [3–9]. Since its first detection in 2008 in the United Kingdom (UK) [4], $M1_{UK}$ has become the dominant *emm*1 genotype isolated from iGAS infections in Australia and the UK [4,6]. $M1_{global}$ and $M1_{UK}$ differ genetically by 27 single nucleotide polymorphisms (SNPs) and 4 indels, with $M1_{UK}$ characterized by upregulated expression of the superantigen Streptococcal pyrogenic exotoxin A (SpeA). In addition, intermediate lineages have been reported carrying 13 of the 27 SNPs found in $M1_{UK}$ [6]. Some $M1_{UK}$ isolates have also been reported to possess additional virulence factors such as the phage-encoded DNase Spd1 and superantigens Streptococcal superantigen (SSA) and Streptococcal pyrogenic exotoxin C (SpeC). The latter have been linked to immune evasion and host colonization in *emm*12 GAS responsible for a surge in scarlet fever cases in Hong Kong in 2011 [6,10–12].

The two-component control of virulence (CovRS) operon consists of a histidine sensor kinase (CovS) and a DNA-binding transcriptional regulator (CovR). The CovRS operon regulates the expression of up to ~15% of the GAS genome and is typically induced during infection, upon exposure to host environmental and immune stress [13,14]. CovR belongs to the OmpR family of bacterial transcriptional response regulators that bind to promoters and other regulatory sites as homodimeric species [15,16]. The formation of these homodimeric species is phosphorylation dependent and occurs following phosphorylation at Asp-53 or Tyr-65 directly by histidine kinases like CovS or through exogenous, low-molecular weight phosphate-donors such as acetyl phosphate [17,18]. Interfacing of CovR homodimers occurs through the CovR receiver domain and is facilitated through the α4-β5-α5 motif. In GAS, this motif is further stabilized by a hydrophobic patch consisting of Val89 (α4), Leu92 (α4), and Ala111 (α5) as well as inter- and intramolecular salt-bridges that further support the hydrophobic patch [19].

Genes encoding several GAS virulence factors, including the hyaluronic acid capsule synthetic operon (*hasABC*), streptodornase I (*sda1*), streptolysin S (*sls*) and O (*slo*), interleukin-8 cleaving enzyme (*spyCEP*), and the streptococcal cysteine protease B (*speB*), are repressed by CovR [20–24]. Mutations in *covRS* have been widely characterized in $M1_{global}$ iGAS and are shown to lead to a hypervirulent phenotype distinguished by ineffective bacterial adherence to epithelial cells, bacterial survival and proliferation in the presence of immune cells, and increased haemolytic activity [14,25–28]. None of the 27 SNPs or indels that distinguish $M1_{UK}$ from $M1_{global}$ occur in the covRS operon. Truncations in *covS* are commonly observed in GAS harbouring *covRS* mutations and prevent phosphorylation of CovR, thereby impeding the phosphorylation-dependent dimerization required to facilitate CovR DNA binding [29]. Mutations in *covR* occur less frequently and tend to be found at nonphosphorylation sites in the receiver domain [30]. This suggests an alternative method for loss of CovR function that does not affect the ability of CovR to be phosphorylated [30]. Furthermore, mutations in *covR* may also impact CovR dimerization and downstream repressor activity.

While the phenotypes of *covRS* mutants are well established for $M1_{global}$ GAS, the recent identification of *covR* and *covS* mutants in $M1_{UK}$ prompts further investigation into the potential compounding effects of *covRS* mutation in an already virulent lineage [4,9,31–33]. Notably, the nonsynonymous CovR^{Ala111Val} mutation was recently identified in $M1_{UK}$, isolated from two separate Australian iGAS clinical isolates [31], with this same mutation previously associated with a fatal infection caused by the GAS *emm*81 genotype [34]. The alanine-to-valine substitution represents a minor biochemical change, and it is unclear how such a change affects the function and structural dynamics of CovR. In this study, we describe the prevalence of *covRS* mutation in the context of *emm*1 iGAS clinical isolates collected in Australia between 2005 and 2023, noting similar rates of mutation in $M1_{UK}$ and $M1_{global}$ isolates. Furthermore, we provide molecular and structural insights into how the CovR^{Ala111Val} mutation at the dimer interface disrupts dimerization, resulting in energetically unfavourable interactions that prevent repression of virulence factors, promoting phenotypes with increased invasive potential.

Experimental procedures

Ethics statement

The study was executed in accordance with the standards set by the Declaration of Helsinki. Experiments involving the use of human blood and neutrophils were conducted with approval from the University of Wollongong Human Research Ethics Committee (Protocol HE08/250). Informed consent was provided by healthy volunteers before donating. The animal model utilized herein was conducted with approval by the University of Queensland Anatomical Biosciences AEC (2021/AE001109).

FEBS Open Bio (2026) © 2026 The Author(s). *FEBS Open Bio* published by John Wiley & Sons Ltd on behalf of Federation of European Biochemical Societies.

22115463, 0, Downloaded from https://febs.onlinelibrary.wiley.com/doi/10.1002/2211-5463.70275 by University Of Technology Sydney, Wiley Online Library on [08/10/2026]. See the Terms and Conditions (https://onlinelibrary.wiley.com/terms-and-conditions) on Wiley Online Library for rules of use; OA articles are governed by the applicable Creative Commons License

Table 1. Bacterial strains and isolates used in this study.

Strain or plasmid	Description	References
Strain		
E. coli Bl21(DE3)pLysS	F- *ompT lon hsd*SB (rB- mB-) *gal dcm* (DE3) pLysS (CamR^{50}, Amp^{100})	Addgene
5448	M1$_{global}$, invasive isolate	[35]
5448AP	5448 with *covS* encoding STOP codon at amino acid (aa) 300	[35]
5448Δ*slo*	5448 Δ*slo::cat*	[36]
5448Δ*speB*	5448 with SpeB deletion	[35]
5448Δ*hasA*	5448 Δ*hasA::cat*	[25]
SP1448	M1$_{UK}$, invasive isolate, *speA*↑	[6]
SP1567	SP1448 with *covS* encoding STOP codon at aa 35	This study
SP1584	SP1448 with *covR* encoding Asp at aa 115	This study
SP1511	M1$_{UK}$, invasive isolate with *covR* encoding Val at aa 111	[31]
SP1512	M1$_{UK}$, invasive isolate with covR encoding Val at aa 111	[31]
Plasmid		
pET19b+	High expression vector, T7lac promoter, adds N-terminal 10x His-tag, Amp^{R}	Addgene
pET19b + -CovR^{WT}	pET19b + with wild-type *covR*	This study
pET19b + -CovR^{Ala111Val}	pET19b + with *covR* encoding Val at aa 111	This study

Bacterial strains, plasmids and culture conditions

Strains and plasmids utilized in this study are outlined in Table 1. GAS strains were routinely streak-purified on horse-blood Columbia agar and liquid cultures grown in Todd Hewitt broth supplemented with 1% yeast extract (THY; Edwards). *Escherichia coli* strain Bl21(DE3)pLysS was used for purification of recombinant CovR^{WT} and CovR^{Ala111Val}. Plasmid selection was performed using 50 μg/mL chloramphenicol and 100 μg/mL ampicillin.

Phylogenetic screening of invasive, Australian, M1$_{UK}$ clinical isolates

Whole genome sequence data representing 374 *emm*1 GAS isolates were collated from Queensland and Victorian public health laboratories (n = 370; 2005–2020 BioProject PRJNA872282), as well as New South Wales and the tropical Top End of the Northern Territory (n = 4 isolates; 2014–2020). This database was processed using snippy v4.6.0 (github/tseemann/snippy) with default parameters to extract SNP core alignments using the MGAS5005 reference genome (NC_007297.2). Recombinant regions within sequences were removed using Gubbins v3.4.0 [37] resulting in an alignment with a total of 792 parsimony-informative SNPs and 1366 singleton sites. The generated alignment was used to construct a maximum-likelihood phylogenetic tree with IQ-TREE v2.4.0. A Hasegawa-Kishino-Yano substitution model with unequal nucleotide frequencies and allowing for a proportion of invariable sites (HKY + F + I) was chosen by ModelFinder according to Bayesian information criterion (BIC). The subsequent tree was visualized using iTOLv6 [38] with MGAS5005 as the outgroup. Lineage-specific differences between the proportion of two-component regulatory gene (*covR* and *covS*) mutations were statistically assessed using a one-tailed proportion test (https://www.socscistatistics.com/tests/ztest/).

In vivo M1$_{UK}$ subcutaneous infection

Ethical approval: All animal procedures were conducted in accordance with the Australian Code for the Care and Use of Animals for Scientific Purposes and approved by the University of Queensland Animal Ethics Committee (approval number: 2021/AE001109).

Animals and housing: Female C57BL/6J mice (6–8 weeks old; Charles River Laboratories, Wilmington, MA, USA) were used in this study. Mice were housed in groups of five under standard conditions (12 h light/dark cycle) with *ad libitum* access to food and water.

Study design and experimental groups: Mice (n = 3) were assigned to a single infection group. No randomization or blinding was performed.

Experimental procedures: Mice were subcutaneously infected with approximately 1×10^{8} colony forming units (CFU) of SP1448 GAS in Dulbecco's PBS (DPBS; no calcium, no magnesium). Mice were monitored daily, and lesions harvested as described previously [20]. Isolated colonies were passaged in THY overnight with supernatants collected and SLO haemolytic and SpeB cysteine protease activity assessed to identify potential *covRS* mutants.

22115463, 0, Downloaded from https://febs.onlinelibrary.wiley.com/doi/10.1002/2211-5463.70275 by University Of Technology Sydney, Wiley Online Library on [08/10/2026]. See the Terms and Conditions (https://onlinelibrary.wiley.com/terms-and-conditions) on Wiley Online Library for rules of use; OA articles are governed by the applicable Creative Commons License

Animal welfare and monitoring: Animal well-being was assessed twice daily throughout the experiment. Humane endpoints were predefined based on clinical signs of severe distress or morbidity. At 3-days postinfection, mice were euthanized by CO_2 inhalation using a controlled chamber.

Outcome measures, sample processing and downstream analysis: Isolated bacterial colonies were passaged overnight in Todd Hewitt yeast extract (THY) broth. Culture supernatants were collected and analysed for streptolysin O (SLO) haemolytic activity and SpeB protease activity.

Sequencing of the *covRS* operon of animal-passaged M1$_{UK}$

In order to sequence the *covRS* operon, genomic DNA was extracted from overnight cultures of select GAS strains using the DNeasy Blood and Tissue Kit (Qiagen, Hilden, Germany) protocol for Gram-positive bacteria. The *covRS* operon was amplified from gDNA using primers P1 (5′-GCTATTCCGGTACAGGTCT-′3) and P12 (5′-TTGCTCTCGTGTGCCATCT-′3) and according to the *PfuUltra* II Fusion HS DNA Polymerase protocol (Agilent) using double the recommended volume of polymerase. Amplified products were run on 1% (w/v) agarose in TAE buffer (40 mM Tris, 20 mM glacial acetic acid, 1 mM EDTA) prestained with GelRed (Biotium) for 1 h at 80 V. In parallel, PCR products were cleaned as per the QIAquick PCR Purification Kit Protocol (Qiagen, Hilden, Germany). Sanger sequencing was performed through the Australian Genome Research Facility and SNPs were detected in *covRS* via alignment against the SP1448 reference genome (GenBank: CP060267.1) in Geneious Prime (version 6.0, Biomatters) software. Whole genome sequencing was performed on four *covRS*-positive mutants and two *covRS*-negative mutants that had apparent *covRS* switching. Individual sequence reads for isolates were mapped to parent strain SP1448 (refseq version, strain ID NZ_CP060267) using breseq version 0.38.1 [39]. High confidence mutations were summarized using gdtools and individual mutations confirmed with assemblies. Assemblies were made using shovill v 1.1.0 (github/tseemann/shovill) with an underlying skesa v 2.5.1 assembler [40].

SpeB cysteine protease activity assay

Overnight GAS cultures were centrifuged at 3220 *g* for 10 min. Culture supernatants and DPBS control were incubated alongside activation buffer [0.1 M sodium acetate (NaAc) (pH 5), 1 mM EDTA, 20 mM DTT] for 1 h at 40 °C. An equal volume of 2% (w/v) azocasein in activation buffer was added to each sample and incubated for another 1 h at 40 °C. Samples were precipitated using 2.5 volumes of 6% (w/v) TCA and immediately centrifuged at 15 000 ***g*** for 5 min. Supernatant turbidity, indicative of azocasein cleavage, was measured spectrophotometrically at 405 nm.

SLO haemolytic assay

Overnight GAS cultures were centrifuged at 3220 *g* for 10 min. In parallel, fresh human peripheral blood was collected in lithium-coated heparin Vacutainers (Interpath, Victoria, Australia) and centrifuged at 500 ***g*** for 10 min and subsequent plasma and buffy coats were aspirated and discarded. Remaining red blood cells (RBCs) were washed with Hanks' Balanced Salt Solution (HBSS; no calcium, no magnesium) and recentrifuged 2–3 times. RBCs were diluted to 2% (v/v) in HBSS and incubated alongside supernatants of each respective GAS strain supernatant, as well as Triton X-100 (1% v/v) and DPBS controls. Samples were incubated for 30 min at 37 °C (5% CO_2). Samples were centrifuged at 1000 ***g*** for 10 min to pellet RBCs, and supernatants were collected. Haemoglobin release was measured spectrophotometrically at 405 nm.

Hyaluronic acid capsule quantification

Hyaluronic acid was purified as per [20] wherein mid-logarithmic GAS cultures (OD_{600} 0.6) were centrifuged at 5000 ***g*** for 5 min and resuspended in 500 µL ultrapure water (UPW). An aliquot of the resuspension was serially diluted in phosphate-buffered saline (PBS) and cultured on THY agar at 37 °C. The remaining volume (400 µL) was placed in 2 mL screw-cap tubes alongside 1 mL chloroform and agitated for 5 min using a Mini-BeadBeater-8 (BioSpec Products, Bartlesville, OK, USA). Homogenates were centrifuged at 13 000 *g* for 10 min and aqueous phases containing hyaluronic acid were collected and stored at 4 °C until quantification. The quantity of hyaluronic acid was determined using a Hyaluronic Acid Test Kit (Corgenix, Broomfield, CO, USA) per manufacturer's instructions and normalized against total bacterial CFU.

Isolation of human neutrophils

Primary human neutrophils were collected as previously described by Williams et al. [28]. Fresh human peripheral blood was collected in lithium-coated heparin Vacutainers (Interpath) and slowly layered on an equal volume of Polymorphprep™ (ProteoGenix,

FEBS Open Bio (2026) © 2026 The Author(s). *FEBS Open Bio* published by John Wiley & Sons Ltd on behalf of Federation of European Biochemical Societies.

22115463, 0, Downloaded from https://febs.onlinelibrary.wiley.com/doi/10.1002/2211-5463.70275 by University Of Technology Sydney, Wiley Online Library on [08/10/2026]. See the Terms and Conditions (https://onlinelibrary.wiley.com/terms-and-conditions) on Wiley Online Library for rules of use; OA articles are governed by the applicable Creative Commons License

Schiltigheim, France) and centrifuged at 500 ***g*** for 35 min with deceleration set to 0. Neutrophils were isolated from their respective layer and contaminating RBCs lysed hypotonically. HBSS was used to restore isotonic conditions. Neutrophils were then resuspended at the desired concentration in complete medium Roswell Park Memorial Institute (RPMI)-1640 medium containing 2 mM L-glutamine and 2% (v/v) heat-inactivated autologous plasma. Neutrophils were maintained at room temperature during handling.

Neutrophil killing assays

Following purification, neutrophil killing of GAS was performed as per Brouwer et al. [11] with minor modifications. Neutrophils were seeded into flat-bottom 96-well plates and infected with GAS strains at an MOI (GAS:neutrophil) of 1 : 10. Cultures were centrifuged at 500 *g* for 5 min to synchronize phagocytosis and incubated for two hours at 37 °C and 5% CO_2. Following infection, neutrophils were lysed by the addition of 0.025% (v/v) Triton X-100 and remaining GAS serially diluted in ultra pure water, plated onto THY agar and incubated at 37 °C. Bacterial survival was calculated as average CFU/mL in coinfected wells over CFU/mL in bacterial alone wells.

AlphaFold CovR protein structure modelling

AlphaFold3 was used to predict the structure of CovR variants using SP1448 CovR as reference for wild-type protein [41]. CovR^{Ala111Val} was generated by substituting valine for alanine-111. CovR variants were modelled as homodimeric species bound to a 23-bp *pho* Box used in the PhoB-DNA crystal structure (1GXP). AlphaFold3 generated CovR variant PDB files were visualized using UCSF ChimeraX 1.8 [42].

Recombinant CovR expression and purification

Cloning pET19b + -CovR^{WT} and pET19b + -CovR^{Ala111Val} was performed through Gene Universal. In brief, sequences for *covR* were sourced from the SP1448 reference genome with CovR^{Ala111Val} generated by changing GCC to GTC in the wild-type sequence to convert Ala to Val at amino acid (aa) 111. Both wild-type and mutant sequences were cloned between the *Nde*I and *Blp*I restriction sites of the pET19b plasmid thereby introducing an enterokinase-cleavable 10x histidine tag on the N-terminal end of each protein. Plasmids were transformed into *Escherichia coli* Bl21(DE3)pLysS and cultured in TYPG medium [1.6% (w/v) tryptone, 1.6% (w/v) yeast extract, 0.5% (w/v) NaCl, 0.25% (w/v) K_2HPO_4, and 0.5% (w/v) glucose] supplemented with ampicillin (100 μg/mL) and chloramphenicol (50 μg/mL) [43]. Bacteria were grown to OD_{600} of 0.8 at 37 °C with agitation wherein cultures were induced with 1 mM isopropyl *β*-D-1-thiogalactopyranoside (IPTG) and incubated for a further four hours at 30 °C. Following incubation, bacteria were harvested via centrifugation at 5000 ***g*** and pellets stored at −20 °C. Cells were lysed per [44] using lysis buffer (50 mM NaH_2PO_4, 0.5 M NaCl, 0.5 mM phenylmethylsulfonyl flouride, 0.5% Tween 20; 4 mL/g pellet) supplemented with lysozyme (1 mg/mL) and incubated for 30 min on ice. Cells were further lysed through five rounds of freeze–thaw and centrifuged at 20 000 *g* for 10 min at 4 °C. Inclusion bodies were collected and solubilized using binding buffer (500 mM NaCl, 20 mM Tris-HCl, 5 mM imidazole, 6 M urea, 5 mL/100 mL original culture volume) and incubated on ice for 1 h and subsequently centrifuged at 16 000 ***g*** (4 °C) for 30 min. Supernatant containing resolubilized protein was filtered through 0.45-μm membranes and incubated with Ni-NTA agarose (1 mL bed volume). Columns were washed with wash buffer (500 mM NaCl, 20 mM Tris-HCl, 60 mM Imidazole, 6 M urea) at 4 °C and proteins eluted with binding buffer containing 500 mM imidazole. Purified protein was refolded and dialysed using storage buffer [50 mM Tris, pH 8.0, 100 mM NaCl, 1 mM EDTA, 20% (v/v) glycerol]. Protein samples were centrifuged again at 20 000 ***g*** (4 °C) for 2 min to remove any aggregates. Throughout lysis and purification, samples were routinely collected and assessed via SDS-PAGE using Tris Glycine eXtended (TGX) stain-free gels (Bio-Rad, Hercules, CA, USA) and visualized using Coomassie blue R250 and Precision Plus™ Protein Dual Colour Standards molecular weight markers (Bio-Rad).

Circular dichroism spectroscopy

CovR secondary structures were assessed following purification and refolding using the Jasco J-810 Spectropolarimeter (Jasco, Tokyo, Japan). CovR variants (200 μL) in 10 mM sodium phosphate buffer (pH 7.4) were loaded into a 0.1 cm pathlength cell and far-UV circular dichroism (CD) spectral data was collected at 37 °C between 190 and 250 nm. A continuous scanning mode was set, with a bandwidth of 1 nm, response time of 2 s and data pitch of 1. Data were collected as an average of six scans, baseline corrected using buffer-only controls and converted to molar residue ellipticity ([θ]) [45]. Determination of relative protein secondary structure abundance was performed by far-UV CD spectra deconvolution using the BeStSel software [46].

22115463, 0, Downloaded from https://febs.onlinelibrary.wiley.com/doi/10.1002/2211-5463.70275 by University Of Technology Sydney, Wiley Online Library on [08/10/2026]. See the Terms and Conditions (https://onlinelibrary.wiley.com/terms-and-conditions) on Wiley Online Library for rules of use; OA articles are governed by the applicable Creative Commons License

In vitro CovR phosphorylation

Prior to phosphorylation, CovR samples were dialysed into phosphorylation buffer PB20 (50 mM Tris, pH 7.4, 50 mM KCl, 20 mM $MgCl_2$). Phosphorylation was performed as previoulsy described [47] and initiated by the addition of phosphomimic lithium potassium acetyl phosphate (LiKAP) (MedChemExpress, Monmouth Junction, NJ, USA) to a final concentration of 50 mM, and CovR (2.85 μM) samples were left to autophosphorylate for 60 min at 37 °C.

Mass photometry

Following phosphorylation, CovR stoichiometry was assessed using mass photometry. Samples were analysed over 10 min at a rate of 600 frames/min with an ONEMP mass photometer (Refeyn LTD, Oxford, UK). Mass photometry experiments were performed in triplicate. Data were obtained and analysed using AquireMP and DiscoverMP, version 1.2.3 (Refeyn LTD) as previously described [48]. Masses were calculated using a standard curve of the ratiometric contrast of proteins of known mass to calculate CovR masses with and without lithium potassium acetyl phosphate (Fig. S2B).

Molecular dynamics simulations

Molecular dynamics (MD) simulations were carried out using Amber22 [49] on NVIDIA Volta or AMD Instinct MI250X GPUs. In total, four systems have been simulated, including CovR^{WT} Rec monomer, CovR^{WT} Rec dimer, CovR^{Ala111Val} Rec monomer and CovR^{Ala111Val} Rec dimer. Initial preparation of systems was done with CHARMM-GUI [50]. The AMBER protein ff14sb force field [51], the TIP3P water model [52] and the Li and Merz 12–6 Ions models [53,54] were applied for protein, water and ions, respectively. Molecular dynamics simulations were performed after solvating the system in a cubic box that extended at least 10 Å from the solute surface. Na^+ and Cl^- counter ions were added to neutralize the system and achieve a salt concentration of 0.15 M. pKa calculations were performed using PROPKA [55,56] to assign protonation states of ionisable residues. Simulations were performed using periodic boundary conditions (PBC) at constant temperature (303.15 K) with the Langevin algorithm (a damping coefficient of 1/ps) and at a pressure of 1.0 bar using the Monte Carlo barostat [57]. The time step was set to 2.0 fs with all covalent bonds involving hydrogens kept rigid with the SHAKE algorithm [58]. Short-range electrostatics were calculated together with long-range electrostatics particle mesh Ewald (PME) with a cut-off of 9.0 Å and a PME grid size of 1.0 Å. For all systems, energy minimization (5000 steps) and 125 ps equilibration were performed first with positional restraints placed on all the protein and DNA heavy atoms (with a force constant of 1.0 kcal/ mol/ Å^2 on the protein atoms). This was followed by 2 or 4 μs production runs. Snapshots were saved every 100 ps. VMD (Visual Molecular Dynamics) [59], LOOS (Lightweight Object-Orientated Structure Analysis) [60,61] and MDAnalysis [62,63] were used to analyse the trajectories.

Free energy calculations

Free energy differences upon Ala111Val mutation on the monomer stability and the dimerization affinity were evaluated with free energy calculations. They were calculated with a double-topology thermodynamic integration. Simulations were set up similar to the MD simulations described above. The time step was set to 1.0 fs with all covalent bonds involving hydrogens kept rigid with the SHAKE algorithm [58] except those involved in the alchemical transformation. The number of λ widows is set to 21, evenly spaced between 0 and 1. The soft-core potential was used to avoid the endpoint catastrophe with scalpha = 0.5, scbeta = 12.0 and gti_add_sc = 5 [64]. The energy terms were saved every 5000 steps for further analysis. Additionally, the relative stabilities were predicted with FoldX (version 5.1) [65] for comparison. In the FoldX calculations, the AlphaFold predicted structures were first repaired and then free energy differences were predicted based on 10 structures of the corresponding wild-type and mutant.

Statistical analyses

All statistical analyses were conducted using Prism software (GraphPad; version 10.6.0). Statistical significance was calculated using ordinary two-way ANOVA and Šídák's *post hoc* analysis or one-way ANOVA using a Holm–Šídák approach for *post hoc*, where defined. *$P < 0.05$, ****$P < 0.0001$.

Results

M1$_{UK}$ isolates acquire *covRS* mutations both clinically and during *in vivo* GAS infection

Given *covRS* mutations are commonly identified in iGAS M1$_{global}$ isolates, we wanted to assess the *covRS*

FEBS Open Bio (2026) © 2026 The Author(s). *FEBS Open Bio* published by John Wiley & Sons Ltd on behalf of Federation of European Biochemical Societies.

22115463, 0, Downloaded from https://febs.onlinelibrary.wiley.com/doi/10.1002/2211-5463.70275 by University Of Technology Sydney, Wiley Online Library on [08/10/2026]. See the Terms and Conditions (https://onlinelibrary.wiley.com/terms-and-conditions) on Wiley Online Library for rules of use; OA articles are governed by the applicable Creative Commons License

mutation frequency in iGAS M1$_{UK}$ isolates in Australia. We performed analysis of 374 Australian GAS *emm*1 isolates using previous genomic data from Queensland and Victorian public health laboratories (n = 370 isolates; 2005–2020), as well as New South Wales and the Northern Territory (n = 4 isolates; 2014–2020) [6,66]. Phylogenetic analysis demonstrated clear separation between M1$_{global}$, M1$_{intermediate}$ and M1$_{UK}$ isolates previously defined in [6]. Mutations in *covRS* did not appear to cluster with any specific clade and were dispersed across both M1$_{global}$ and M1$_{UK}$ lineages (Fig. 1A). Further analysis of the *covRS* operon demonstrated that frequencies of SNPs in regulatory genes *covR* and *covS* were not significantly different between M1$_{global}$ (2.7% and 7.6%, respectively) and M1$_{UK}$ (3.3% and 4.4%, respectively) (one-tailed proportion test: *covR* P-value > 0.05; *covS* P-value > 0.05) (Fig. 1B). Notably, mutations in *covR* were exclusively nonsynonymous, while *covS* mutations were predominantly truncations (Fig. 1B).

Next, we assessed whether *covRS* mutation could be replicated through *in vivo* passage of the invasive M1$_{UK}$ isolate SP1448 using a subcutaneous murine infection model (Fig. S1A) [20]. Animal-passaged (AP) isolates were screened for characteristic *covRS* mutant phenotypes wherein 35.5% exhibited increased SLO haemolytic activity, while 43.3% showed a reduction in SpeB protease activity (Fig. S1B,C). Fifteen isolates with the highest SLO activity were selected for sequencing of the *covRS* operon. Mutations in both *covR* and *covS* were identified in 40% (6/15) of selected isolates. Two representative AP M1$_{UK}$ strains containing *covR* and *covS* mutations were selected for further characterization. These included SP1584 containing a CovR^{Ala115Asp} substitution located proximally to the previously reported Ala111Val substitution in M1$_{UK}$ isolates SP1511/SP1512 [31] and SP1567 containing a CovS truncation at amino acid residue 35 identical to previously screened M1$_{UK}$ clinical isolates [6]. Whole genome sequence analysis of these isolates confirmed the absence of additional mutations (Table S1). Combined, these data confirm the ability of M1$_{UK}$ GAS to acquire mutations in *covRS* using a murine model of GAS infection and in similar locations observed in M1$_{global}$.

To confirm the functional impact of *covRS* mutations in M1$_{UK}$ GAS, we assessed common virulence phenotypes in clinical and AP *covRS* mutant isolates. Compared to wild-type M1$_{UK}$, both AP (SP1567 and SP1584) and clinically derived CovR^{Ala111Val}-mutant (SP1511 and SP1512) isolates exhibited significantly elevated SLO activity and decreased SpeB protease activity (P < 0.0001) (Fig. 1C,D), consistent with M1$_{global}$ *covRS* mutants (5448AP). Additionally, significantly increased production of hyaluronic acid capsules was exhibited for both AP and CovR^{Ala111Val}-M1$_{UK}$ isolates when compared to wild-type M1$_{UK}$ (P < 0.0001) (Fig. 1E). We next assessed GAS survival in the presence of human neutrophils. CovR^{Ala111Val} and AP M1$_{UK}$ isolates showed resistance to neutrophil mediated killing compared to wild-type M1$_{UK}$ (P < 0.05) (Fig. 1F), as has been shown for M1$_{global}$ *covRS* mutants.

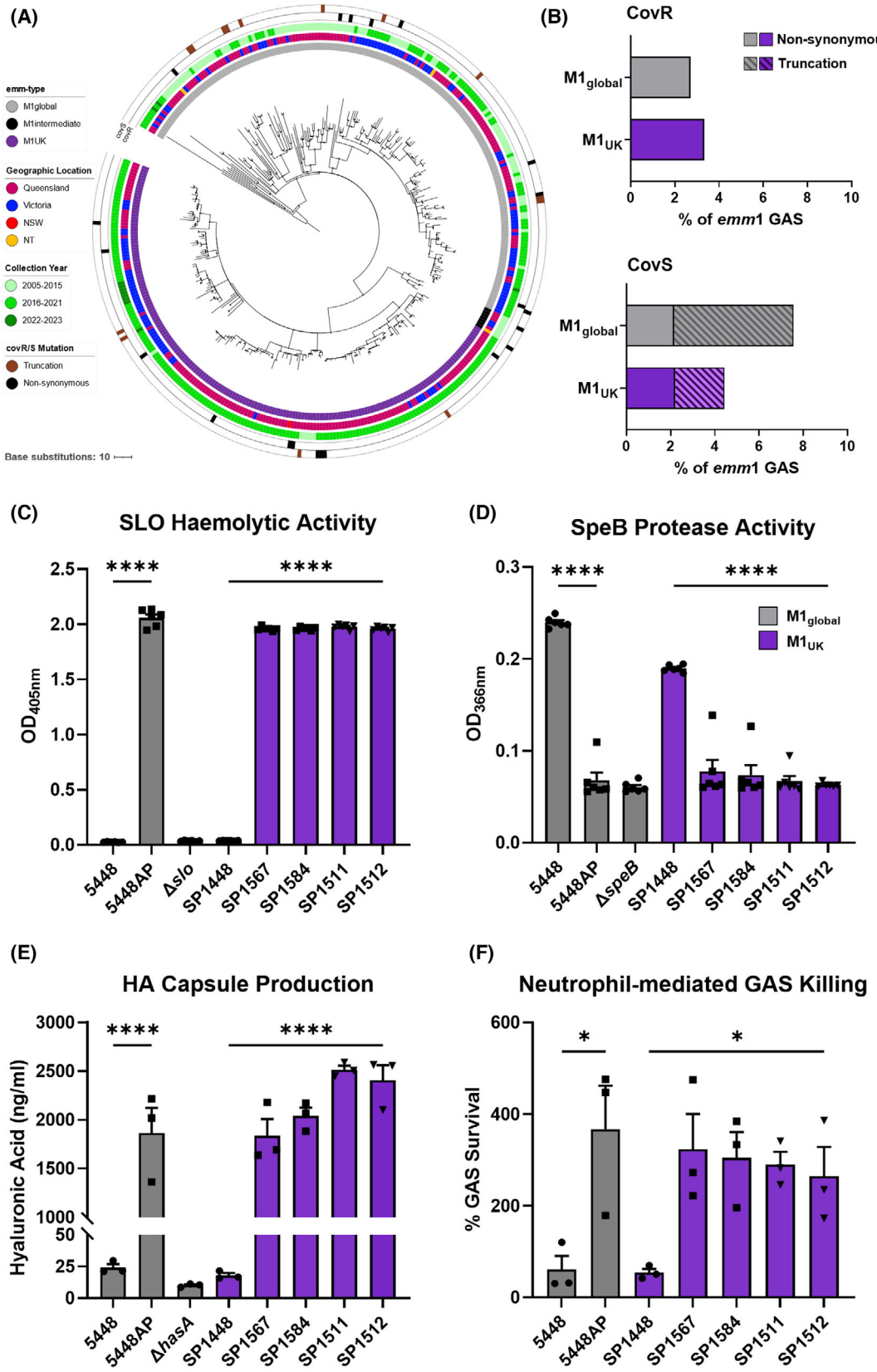
Ala111Val affects formation of CovR secondary structures, destabilizes CovR dimers and impacts phosphorylation-dependent dimerization

Recently, an Ala111Val substitution in CovR was reported in invasive clinical M1$_{UK}$ isolates SP1511 and SP1512, and in a previously fatal strain of *emm*81 GAS [31,34]. Upon dimerization, the CovR homodimer is stabilized through interfacing residues and hydrophobic patches in the receiver (REC) domain, where the Ala111Val mutation is situated. An alanine-to-valine substitution represents a minor biochemical change, and as such, we sought to characterize how this change affects CovR structural dynamics. We first modelled the complex formed between dimeric SP1448 CovR^{WT} and CovR^{Ala111Val} subunits bound to 23-bp *pho* box DNA using AlphaFold3. This revealed that the Ala111Val substitution occurs in the α4-β5-α5 motif, a critical region of the CovR dimer interface. Specifically, Ala111Val is positioned within the α4 helix and contributes to a hydrophobic patch formed alongside Val89 and Leu92 (Fig. 2A). The substitution of Ala with a slightly bulkier Val residue was predicted to destabilize CovR secondary and quaternary structures.

Firstly, we assessed secondary structures using CD spectroscopy of purified recombinant CovR^{WT} and CovR^{Ala111Val} (Fig. S2A). For both CovR variants, far-UV CD spectra demonstrated distinct minima at 208 nm and 222 nm and maxima at 190 nm. However, CovR^{Ala111Val} showed less pronounced minima at 208 and 222 nm compared to CovR^{WT} (Fig. 2B). Using BeStSel software [46], far-UV CD spectra were deconvoluted to assess the proportion of secondary structures including α-helices, β-sheets and turns. There were no significant differences in the proportion of β-sheets or turns between the CovR variants; however, CovR^{Ala111Val} had a significantly lower proportion of α-helical structures (14.9% ± 0.29) compared to CovR^{WT} (23.9% ± 0.87) (mean ± SEM) (P < 0.0001) (Fig. 2C).

Next, we characterized how the Ala111Val substitution impacts CovR dimerization using *in silico*,

22115463, 0, Downloaded from https://febs.onlinelibrary.wiley.com/doi/10.1002/2211-5463.70275 by University Of Technology Sydney, Wiley Online Library on [08/10/2026]. See the Terms and Conditions (https://onlinelibrary.wiley.com/terms-and-conditions) on Wiley Online Library for rules of use; OA articles are governed by the applicable Creative Commons License



FEBS Open Bio (2026) © 2026 The Author(s). *FEBS Open Bio* published by John Wiley & Sons Ltd on behalf of Federation of European Biochemical Societies.

22115463, 0, Downloaded from https://febs.onlinelibrary.wiley.com/doi/10.1002/2211-5463.70275 by University Of Technology Sydney, Wiley Online Library on [08/10/2026]. See the Terms and Conditions (https://onlinelibrary.wiley.com/terms-and-conditions) on Wiley Online Library for rules of use; OA articles are governed by the applicable Creative Commons License

Fig. 1. M1$_{UK}$ acquires *covRS* mutations in clinical and *in vivo* contexts and exhibits *in vitro* phenotypes characteristic of hypervirulent M1$_{global}$ GAS. (A) Maximum-likelihood phylogenetic analysis built on 792 core SNPs extracted from 374 invasive *emm*1 isolates mapped to MGAS5005 (NC_007297.2). Isolates were collected in Australia (Victorian, Queensland, New South Wales and Northern Territory) between 2005 and 2023. Black circles represent branches with > 90% bootstrap support and external rings indicate isolate *emm*-type, location, year and presence of *covR/S* mutations. (B) Frequency of *covR* and *covS* mutations in M1$_{global}$ (grey; *covR* 5/185, *covS* 14/185) and M1$_{UK}$ (purple; *covR* 6/180, *covS* 8/180) clinical isolates (one-tailed proportion test: *covR P*-value > 0.05; *covS P*-value > 0.05). SNP type is denoted as solid bars (nonsynonymous) or diagonal bars (truncated). (C,D) SLO haemolytic and SpeB protease activity measured spectrophotometrically via haemoglobin release (405 nm) and azocasein cleavage (366 nm). (E) Hyaluronic acid capsule production in mid-logarithmic GAS. (F) GAS survival after exposure to human neutrophils ($n = 3$ donors) assessed as percent bacterial survival in comparison to inoculum. Panels A,B show mean ± SEM ($n = 6$), representing three independent experiments. Panels C,D show pooled means ± SEM ($n = 3$ independent experiments). Animal-passaged (AP) GAS (■), clinical GAS isolates (●), clinically derived M1$_{UK}$ containing CovR^{Ala111Val} (▼). One-way ANOVA was performed for all panels using the Holm-Šídák approach for *post hoc* analyses against each lineage's wild-type (WT) counterpart. *$P < 0.05$ and ****$P < 0.0001$. HA, hyaluronic acid, TX-100, Triton X-100, SLO, Streptolysin O, AP, animal passaged, SpeB, Streptococcal pyrogenic exotoxin B.

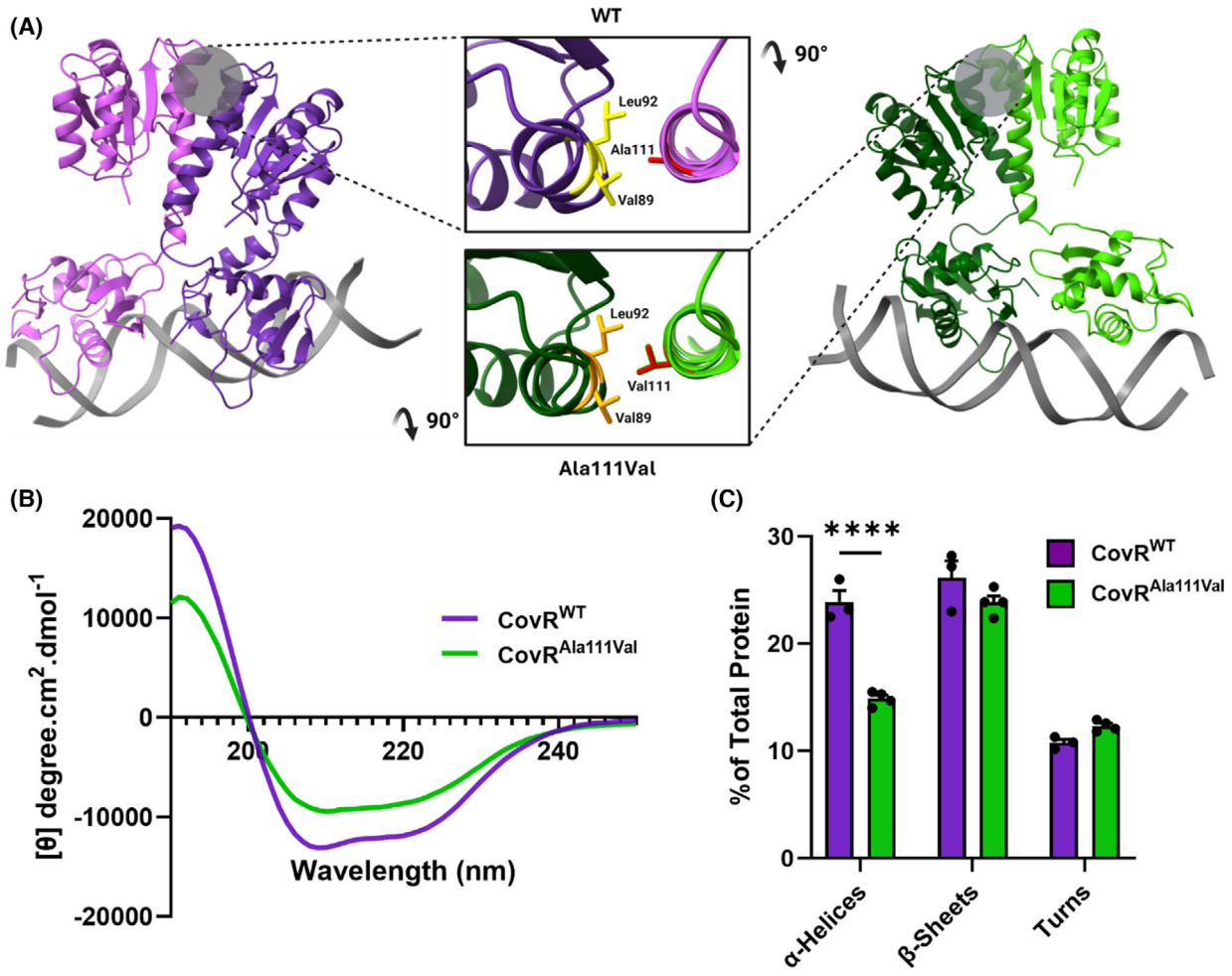


Fig. 2. Ala111Val destabilizes CovR secondary structures. (A) AlphaFold3 modelling of CovR^{WT} (purple) and CovR^{Ala111Val} (green) as homodimeric units bound to 23-bp *pho* Box (grey) used in PhoB-DNA crystal structure (PDB id: 1GXP). (B) Circular dichroism (CD) spectra of recombinant CovR analysed under continuous scanning mode at 37 °C. (C) Comparative secondary structure predictions shown by deconvolution of far-UV CD spectra in (B). Results represent the mean ± SEM of four individual scans each recorded in triplicate corrected against a buffer-only control (B). Results represent the mean ± SEM of at least 3 deconvoluted CD spectra using BeStSel software (C). Significance was determined using ordinary two-way ANOVA and Šídák's approach *post hoc* analysis. ****$P < 0.0001$. Figure 2A created with BioRender.com.

22115463, 0, Downloaded from https://febs.onlinelibrary.wiley.com/doi/10.1002/2211-5463.70275 by University Of Technology Sydney, Wiley Online Library on [08/10/2026]. See the Terms and Conditions (https://onlinelibrary.wiley.com/terms-and-conditions) on Wiley Online Library for rules of use; OA articles are governed by the applicable Creative Commons License

thermodynamic integration simulation of Ala to Val in the REC domain of monomeric and dimeric forms of CovR^{WT} and CovR^{Ala111Val}. The Ala111Val mutation notably destabilized dimerization of CovR by 3.8 kcal/mol (Table S2). MD simulations revealed increased root mean square fluctuation (RMSF) values, indicative of enhanced Cα atom flexibility at interfacing residues 80–90 in one subunit of CovR^{Ala111Val} compared to CovR^{WT} (Figure S3F). Across all simulations, both CovR variants remained stable with consistent RMSD values (Tables S3 and S4, Fig. S3A–D). Combined with CD, these data suggest that the Ala111Val mutation results in energetic destabilization of CovR monomers, the CovR dimer interface region and a reduction in overall helical content, potentially affecting the ability of CovR to undergo dimerization.

We next validated how Ala111Val affected the phosphorylation-dependent dimerization of recombinant CovR using mass photometry. This was performed following treatment of CovR variants with LiKAP, a high-energy phosphate donor that mimics endogenous bacterial acetyl phosphate that, alongside CovS, can also promote phosphorylation-dependent dimerization [47]. Prior to phosphorylation, CovR^{WT} was shown to exist as a single monomeric species (~30 kDa), in line with its predicted mass (Figs 3A and S2A). Following incubation with LiKAP, the mass of CovR^{WT} shifted to ~65 kDa suggesting the formation of a dimeric species (Fig. 3B). However, CovR^{Ala111Val} remained monomeric before and after LiKAP treatment (Fig. 3B), confirming that the Ala111Val mutation alters the ability of CovR to undergo dimerization.

Discussion

The resurgence of iGAS pathologies has been partly attributed to the emergence of the M1$_{UK}$ lineage. GAS virulence is heavily regulated by several endogenous regulatory pathways, notably two-component regulatory systems, including CovRS. Acquisition of spontaneous mutations in *covRS* during infection can generate hypervirulent strains of GAS, increasing the severity of disease [67,68]. While mutations in *covRS* have been extensively characterized in the M1$_{global}$ lineage, their prevalence and functional impact have been less extensively studied in M1$_{UK}$.

In this study, we noted similar proportions of *covRS* mutation in clinical M1$_{global}$ and M1$_{UK}$ iGAS, and confirmed the ability of M1$_{UK}$ GAS to acquire *covRS* mutations in a subcutaneous mouse model of infection. Mutations in *covS* were more common in both clinical and AP isolates and were composed of both nonsynonymous and frameshift mutations, as has been previously reported [29]. In the present study, we observed expected phenotypes associated with mutations in *covRS* for all M1$_{UK}$ strains, including decreased SpeB expression, increased expression of hyaluronic acid capsule and increased SLO activity, as well as an increased ability to survive in the presence of neutrophils, as previously observed for M1$_{global}$ GAS [20,25,27,33,69].

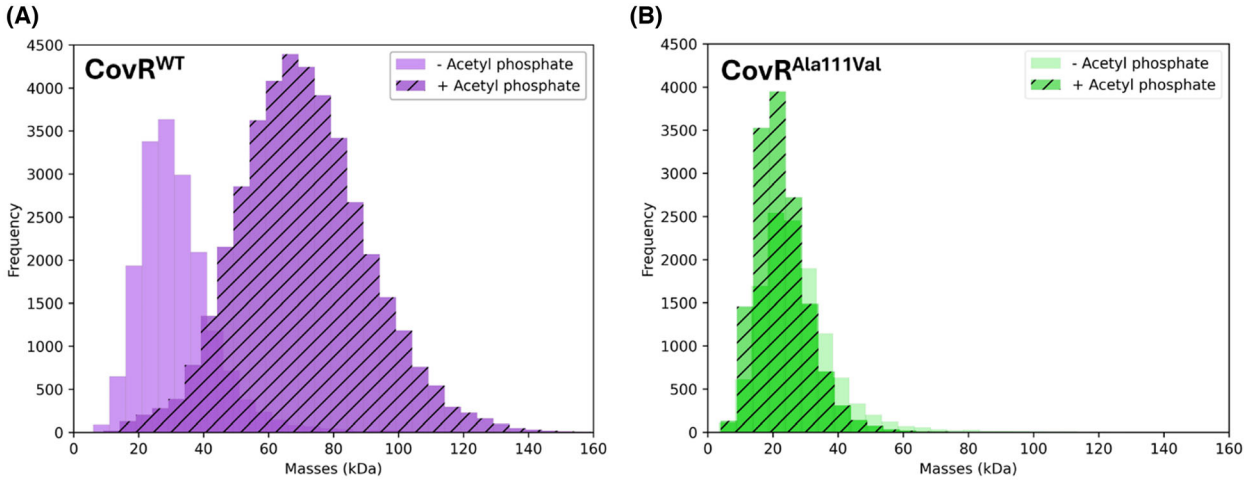


Fig. 3. Ala111Val alters CovR stoichiometry following treatment with lithium potassium acetyl phosphate (LiKAP). CovR^{WT} (A) and CovR^{Ala111Val} (B) at 2.85 μM were artificially phosphorylated using a high-energy phosphomimic LiKAP (28 mM) in PB20 buffer for 60 min at 37 °C and directly analysed via mass photometry. Analysis of (A) recombinant CovR^{WT} treated with LiKAP (purple, diagonal lines) demonstrates a mass distribution shift that is absent in (B) CovR^{Ala111Val} also treated with LiKAP (green, diagonal lines). Histograms represent pooled data from three independent experiments.

FEBS Open Bio (2026) © 2026 The Author(s). *FEBS Open Bio* published by John Wiley & Sons Ltd on behalf of Federation of European Biochemical Societies.

22115463, 0, Downloaded from https://febs.onlinelibrary.wiley.com/doi/10.1002/2211-5463.70275 by University Of Technology Sydney, Wiley Online Library on [08/10/2026]. See the Terms and Conditions (https://onlinelibrary.wiley.com/terms-and-conditions) on Wiley Online Library for rules of use; OA articles are governed by the applicable Creative Commons License

covR mutations in M1$_{UK}$ GAS were rarer than *covS* mutations and were mainly represented by nonsynonymous mutations, consistent with previous studies [29]. Specifically, we investigated two M1$_{UK}$ isolates from invasive infections containing a *covR* mutation encoding CovR^{Ala111Val} [31]. While the Ala111Val substitution in CovR is not novel, its impact on CovR structural dynamics remains poorly understood. Previous work demonstrated that CovR^{Ala111Val} found in a strain of *emm*81 GAS associated with rapidly progressive lethal necrotizing fasciitis exhibited poor phosphorylation-dependent binding to virulence factor promoters [34]. However, given CovR binds to promoter sequences as a homodimer, we hypothesized that Ala111Val mediated disruption of dimerization may also contribute to *covRS* dysregulation. Given that Ala111Val resides in the hydrophobic patch of the CovR dimer interface, we proposed that its introduction may specifically alter dimer stability [19]. Molecular dynamics simulations, in conjunction with free energy calculation, demonstrated clear displacement of interfacing amino acid residues (80–90) in CovR^{Ala111Val} which likely resulted in the observed energetic destabilization at the dimer interface. However, the simulations revealed asymmetric fluctuations at the mutation site between the two monomers, with pronounced RMSF increases around the interfacing residues observed only in one subunit. This suggests that the system may have adapted to the perturbation in a nonsymmetric manner, potentially reflecting differential local responses to the mutation. We note that phosphorylation was not directly confirmed for either CovR^{WT} or CovR^{Ala111Val} following LiKAP treatment. Further investigation is therefore warranted to determine whether the secondary structure alterations observed herein influence the phosphorylation of CovR^{Ala111Val}.

Herein, we have shown that the Ala111Val mutation reduces the proportion of α-helices in CovR monomers. This is consistent with the fact that of the four aliphatic amino acids, valine is a weak α-helix destabilizer [70]. Taken together, the position of the Ala111Val mutation in the α5 helix of the α4-β5-α5 interfacing motif may affect the hydrophobic patch, allowing valine-89 and leucine-92 greater mobility, likely contributing to the higher RMSF values observed in MD simulations. Finally, we have shown through mass photometry that phosphorylation-dependent dimerization was significantly diminished for CovR^{Ala111Val}, likely due to the aforementioned conformation changes and energetically unfavourable interactions at the CovR dimer interface.

In this study, we confirm that the M1$_{UK}$ lineage of GAS can acquire mutations in the *covRS* regulatory system both in clinical isolates and though passage in a murine model of infection. We further demonstrate that the Ala111Val mutation in CovR disrupts monomeric secondary structures, destabilizes the dimer interface, and impairs phosphorylation-dependent dimerization. Ala111Val has previously been shown to prevent phosphorylation-dependent binding of CovR to key GAS virulence factor promoters requiring homodimeric CovR. We propose that this loss of binding results from a reduced ability of CovR^{Ala111Val} to dimerize. Although *covRS* mutations are relatively rare, they can significantly alter CovR and CovS protein function, leading to enhanced bacterial virulence. The identification of such mutations within the already hypervirulent M1$_{UK}$ lineage underscores the need for ongoing epidemiological surveillance.

Acknowledgements

This research was supported by the National Health and Medical Research Council of Australia GNT2019767 (MSS, SB, JT). Parts of this research were supported by the ARC Centre of Excellence in Quantum Biotechnology through project number CE230100021 (HY). This work was supported with computational resources provided by the Australian Government through the National Computational Infrastructure National Facility and the Pawsey Supercomputer Centre. JDP is the recipient of an Australian Postgraduate Award. We also thank Dr. Aidan Grosas for his invaluable discussions on initial attempts at simulating CovR dimer structures.. Open access publishing facilitated by University of Wollongong, as part of the Wiley - University of Wollongong agreement via the Council of Australasian University Librarians

Conflict of interest

The authors declare no conflicts of interest.

Author contributions

MD, MJW, MSS and SB conceived and designed the study. AH, EJP, JP, JW, NPJ and SB performed the experiments. AH, EJP, GM, HY, JP, JW, MD, MJW, MSS, NPJ and SB analysed and interpreted the data. MJW, MSS and SB provided materials and reagents. JP wrote the original draft of the manuscript. EJP, GM, HY, JT, MJW, MRD, MSS, NPJ, RS and SB reviewed and edited the manuscript. HY, JT, MJW, MSS and SB acquired funding for respective parts of the project. EJP, HY, MD, MSS, RS and SB supervised the study.

22115463, 0, Downloaded from https://febs.onlinelibrary.wiley.com/doi/10.1002/2211-5463.70275 by University Of Technology Sydney, Wiley Online Library on [08/10/2026]. See the Terms and Conditions (https://onlinelibrary.wiley.com/terms-and-conditions) on Wiley Online Library for rules of use; OA articles are governed by the applicable Creative Commons License

Data availability statement

The sequence data that support the findings of this study are openly available at NCBI BioProject PRJNA872282. The DNA sequence found within the PhoB-DNA crystal structure (PDB: 1GXP) used in this study was obtained from the Protein Data Bank (https://www.rcsb.org/structure/1GXP). AlphaFold3 generated CovR variant PDB files are available from the corresponding author (martina@uow.edu.au) upon reasonable request. Supporting data are also available in the supporting information of this article.

References

1 Walker MJ, Barnett TC, Mcarthur JD, Cole JN, Gillen CM, Henningham A, Sriprakash KS, Sanderson-Smith ML and Nizet V (2014) Disease manifestations and pathogenic mechanisms of group A streptococcus. *Clin Microbiol Rev* **27**, 264–301.

2 Carapetis JR, Steer AC, Mulholland EK and Weber M (2005) The global burden of group A streptococcal diseases. *Lancet Infect Dis* **5**, 685–694.

3 Lynskey NN, Jauneikaite E, Li HK, Zhi X, Turner CE, Mosavie M, Pearson M, Asai M, Lobkowicz L, Chow JY *et al.* (2019) Emergence of dominant toxigenic M1T1 streptococcus pyogenes clone during increased scarlet fever activity in England: a population-based molecular epidemiological study. *Lancet Infect Dis* **19**, 1209–1218.

4 Vieira A, Wan Y, Ryan Y, Li HK, Guy RL, Papangeli M, Huse KK, Reeves LC, Soo VWC, Daniel R *et al.* (2024) Rapid expansion and international spread of M1UK in the post-pandemic UK upsurge of streptococcus pyogenes. *Nat Commun* **15**, 3916.

5 Cipolla L, Gianecini A, Poklepovich T, Etcheverry P, Rocca F and Prieto M (2025) Genomic epidemiology of invasive group A streptococcus infections in Argentina, 2023: high prevalence of emm1-global and detection of emm1 hypervirulent lineages. *Microbiol Spectrum* **13**, e0131024.

6 Davies MR, Keller N, Brouwer S, Jespersen MG, Cork AJ, Hayes AJ, Pitt ME, DE Oliveira DMP, HARBISON-Price N, Bertolla OM *et al.* (2023) Detection of streptococcus pyogenes M1UK in Australia and characterization of the mutation driving enhanced expression of superantigen SpeA. *Nat Commun* **14**, 1051.

7 Demczuk W, Martin I, Domingo FR, Macdonald D and Mulvey MR (2019) Identification of streptococcus pyogenes M1UK clone in Canada. *Lancet Infect Dis* **19**, 1284–1285.

8 Matsui Y, Mizuno S, Anraku M, Yamaguchi T, Sugino M, Kawahara R and Kasai M (2025) Clinical and microbiological characterization of invasive group a streptococcus infection in children in Japan: A single-center experience. *J Infect Chemother* **31**, 102560.

9 Rümke LW, DE Gier B, Vestjens SMT, Van Der Ende A, VAN Sorge NM, Vlaminckx BJM, Witteveen S, VAN Santen M, Schouls LM and Kuijper EJ (2020) Dominance of M1(UK) clade among Dutch M1 streptococcus pyogenes. *Lancet Infect Dis* **20**, 539–540.

10 Davies MR, Mcintyre L, Mutreja A, Lacey JA, Lees JA, Towers RJ, Duchêne S, Smeesters PR, Frost HR, Price DJ *et al.* (2019) Atlas of group A streptococcal vaccine candidates compiled using large-scale comparative genomics. *Nat Genet* **51**, 1035–1043.

11 Brouwer S, Barnett TC, Ly D, Kasper KJ, DE Oliveira DMP, Rivera-Hernandez T, Cork AJ, Mcintyre L, Jespersen MG, Richter J *et al.* (2020) Prophage exotoxins enhance colonization fitness in epidemic scarlet fever-causing streptococcus pyogenes. *Nat Commun* **11**, 5018.

12 Zhi X, Li HK, Li H, Loboda Z, Charles S, Vieira A, Huse K, Jauneikaite E, Reeves L, Mok K *et al.* (2023) Emerging invasive group A streptococcus M1UK lineage detected by allele-specific Pcr, England, 2020. *Emerging Infectious Disease Journal* **29**, 1007.

13 Graham MR, Smoot LM, Migliaccio CA, Virtaneva K, Sturdevant DE, Porcella SF, Federle MJ, Adams GJ, Scott JR and Musser JM (2002) Virulence control in group A streptococcus by a two-component gene regulatory system: global expression profiling and in vivo infection modeling. *Proc Natl Acad Sci USA* **99**, 13855–13860.

14 Sumby P, Whitney AR, Graviss EA, Deleo FR and Musser JM (2006) Genome-wide analysis of group A streptococci reveals a mutation that modulates global phenotype and disease specificity. *PLoS Pathog* **2**, e5.

15 Mazzuoli MV, Daunesse M, Varet H, Rosinski-Chupin I, Legendre R, Sismeiro O, Gominet M, Kaminski PA, Glaser P, Chica C *et al.* (2021) The CovR regulatory network drives the evolution of group B streptococcus virulence. *PLoS Genet* **17**, e1009761.

16 Wang S (2012) Bacterial two-component systems: structures and signaling mechanisms. In *Protein Phosphorylation in Human Health* (Huang C, ed). IntechOpen, Rijeka.

17 Horstmann N, Saldaña M, Sahasrabhojane P, Yao H, Su X, Thompson E, Koller A and Shelburne SA III (2014) Dual-site phosphorylation of the control of virulence regulator impacts group A streptococcal global gene expression and pathogenesis. *PLoS Pathog* **10**, e1004088.

18 Plainvert C, Rosinski-Chupin I, Weckel A, Lambert C, Touak G, Sauvage E, Poyart C, Glaser P and Fouet A (2023) A novel CovS variant harbored by a colonization strain reduces streptococcus pyogenes virulence. *J Bacteriol* **205**, e00039.

FEBS Open Bio (2026) © 2026 The Author(s). *FEBS Open Bio* published by John Wiley & Sons Ltd on behalf of Federation of European Biochemical Societies.

22115463, 0, Downloaded from https://febs.onlinelibrary.wiley.com/doi/10.1002/2211-5463.70275 by University Of Technology Sydney, Wiley Online Library on [08/10/2026]. See the Terms and Conditions (https://onlinelibrary.wiley.com/terms-and-conditions) on Wiley Online Library for rules of use; OA articles are governed by the applicable Creative Commons License

19 Toro-Roman A, Mack TR and Stock AM (2005) Structural analysis and solution studies of the activated regulatory domain of the response regulator ArcA: a symmetric dimer mediated by the alpha4-beta5-alpha5 face. *J Mol Biol* **349**, 11–26.
20 Cole JN, Pence MA, Von Köckritz-Blickwede M, Hollands A, Gallo RL, Walker MJ and Nizet V (2010) M protein and hyaluronic acid capsule are essential for in vivo selection of covRS mutations characteristic of invasive serotype M1T1 group A streptococcus. *MBio* **1**, e00191.
21 Heath A, Dirita VJ, Barg NL and Engleberg NC (1999) A two-component regulatory system, CsrR-CsrS, represses expression of three streptococcus pyogenes virulence factors, hyaluronic acid capsule, streptolysin S, and pyrogenic exotoxin B. *Infect Immun* **67**, 5298–5305.
22 Jain I, Danger JL, Burgess C, Uppal T and Sumby P (2020) The group A streptococcus accessory protein RocA: regulatory activity, interacting partners and influence on disease potential. *Mol Microbiol* **113**, 190–207.
23 Shelburne SA, Olsen RJ, Suber B, Sahasrabhojane P, Sumby P, Brennan RG and Musser JM (2010) A combination of independent transcriptional regulators shapes bacterial virulence gene expression during infection. *PLoS Pathog* **6**, e1000817.
24 Treviño J, Perez N, Ramirez-Peña E, Liu Z, Shelburne SA 3rd, Musser JM and Sumby P (2009) CovS simultaneously activates and inhibits the CovR-mediated repression of distinct subsets of group A streptococcus virulence factor-encoding genes. *Infect Immun* **77**, 3141–3149.
25 Hollands A, Pence MA, Timmer AM, Osvath SR, Turnbull L, Whitchurch CB, Walker MJ and Nizet V (2010) Genetic switch to Hypervirulence reduces colonization phenotypes of the globally disseminated group A streptococcus M1T1 clone. *J Infect Dis* **202**, 11–19.
26 Maamary PG, Sanderson-Smith ML, Aziz RK, Hollands A, Cole JN, Mckay FC, Mcarthur JD, Kirk JK, Cork AJ, Keefe RJ *et al.* (2010) Parameters governing invasive disease propensity of non-M1 serotype group A streptococci. *J Innate Immun* **2**, 596–606.
27 Walker MJ, Hollands A, Sanderson-Smith ML, Cole JN, Kirk JK, Henningham A, Mcarthur JD, Dinkla K, Aziz RK, Kansal RG *et al.* (2007) DNase Sda1 provides selection pressure for a switch to invasive group A streptococcal infection. *Nat Med* **13**, 981–985.
28 Williams JG, Ly D, Geraghty NJ, Mcarthur JD, Vyas HKN, Gorman J, Tsatsaronis JA, Sluyter R and Sanderson-Smith ML (2020) Streptococcus pyogenes M1T1 variants induce an inflammatory neutrophil phenotype including activation of inflammatory caspases. *Front Cell Infect Microbiol* **10**, 596023.
29 Friães A, Pato C, Melo-Cristino J and Ramirez M (2015) Consequences of the variability of the CovRS and RopB regulators among streptococcus pyogenes causing human infections. *Sci Rep* **5**, 12057.
30 Horstmann N, Sahasrabhojane P, Suber B, Kumaraswami M, Olsen RJ, Flores A, Musser JM, Brennan RG and Shelburne SA III (2011) Distinct single amino acid replacements in the control of virulence regulator protein differentially impact streptococcal pathogenesis. *PLoS Pathog* **7**, e1002311.
31 Brouwer S, Das S, Hayes AJ, Bertolla OM, Davies MR, Walker MJ, Whiley DM, Irwin AD and Tickner JA (2024) A rapid molecular detection tool for toxigenic M1UK streptococcus pyogenes. *J Infect Dis* **231**, e375–e384.
32 Li HK, Zhi X, Vieira A, Whitwell HJ, Schricker A, Jauneikaite E, Li H, Yosef A, Andrew I, Game L *et al.* (2023) Characterization of emergent toxigenic $M1_{UK}$ *Streptococcus pyogenes* and associated sublineages. *Microbial Genomics* **9**, mgen000994.
33 Richter J, Cork AJ, Ong Y, Keller N, Hayes AJ, Schembri MA, Jennison AV, Davies MR, Schroder K, Walker MJ *et al.* (2025) Characterization of a novel covS SNP identified in Australian group A streptococcus isolates derived from the M1(UK) lineage. *MBio* **16**, e0336624.
34 Turner CE, Kurupati P, Jones MD, Edwards RJ and Sriskandan S (2009) Emerging role of the interleukin-8 cleaving enzyme SpyCEP in clinical streptococcus pyogenes infection. *J Infect Dis* **200**, 555–563.
35 Aziz RK, Pabst MJ, Jeng A, Kansal R, Low DE, Nizet V and Kotb M (2004) Invasive M1T1 group A streptococcus undergoes a phase-shift in vivo to prevent proteolytic degradation of multiple virulence factors by SpeB. *Mol Microbiol* **51**, 123–134.
36 Timmer AM, Timmer JC, Pence MA, Hsu LC, Ghochani M, Frey TG, Karin M, Salvesen GS and Nizet V (2009) Streptolysin O promotes group A streptococcus immune evasion by accelerated macrophage apoptosis. *J Biol Chem* **284**, 862–871.
37 Croucher NJ, Page AJ, Connor TR, Delaney AJ, Keane JA, Bentley SD, Parkhill J and Harris SR (2014) Rapid phylogenetic analysis of large samples of recombinant bacterial whole genome sequences using Gubbins. *Nucleic Acids Res* **43**, e15.
38 Letunic I and Bork P (2024) Interactive Tree of life (iTOL) v6: recent updates to the phylogenetic tree display and annotation tool. *Nucleic Acids Res* **52**, W78–W82.
39 Deatherage DE and Barrick JE (2014) Identification of mutations in laboratory-evolved microbes from next-generation sequencing data using breseq. In *Engineering and Analyzing Multicellular Systems: Methods and Protocols* (Sun L and Shou W, eds). Springer New York, New York, NY.

22115463, 0, Downloaded from https://febs.onlinelibrary.wiley.com/doi/10.1002/2211-5463.70275 by University Of Technology Sydney, Wiley Online Library on [08/10/2026]. See the Terms and Conditions (https://onlinelibrary.wiley.com/terms-and-conditions) on Wiley Online Library for rules of use; OA articles are governed by the applicable Creative Commons License

40 Souvorov A, Agarwala R and Lipman DJ (2018) SKESA: strategic k-mer extension for scrupulous assemblies. *Genome Biol* **19**, 153.
41 Abramson J, Adler J, Dunger J, Evans R, Green T, Pritzel A, Ronneberger O, Willmore L, Ballard AJ, Bambrick J *et al*. (2024) Accurate structure prediction of biomolecular interactions with AlphaFold 3. *Nature* **630**, 493–500.
42 Meng EC, Goddard TD, Pettersen EF, Couch GS, Pearson ZJ, Morris JH and Ferrin TE (2023) UCSF ChimeraX: tools for structure building and analysis. *Protein Sci* **32**, e4792.
43 Federle MJ and Scott JR (2002) Identification of binding sites for the group A streptococcal global regulator CovR. *Mol Microbiol* **43**, 1161–1172.
44 Miller AA, Engleberg NC and Dirita VJ (2001) Repression of virulence genes by phosphorylation-dependent oligomerization of CsrR at target promoters in S. Pyogenes. *Mol Microbiol* **40**, 976–990.
45 Greenfield NJ (2006) Using circular dichroism spectra to estimate protein secondary structure. *Nat Protoc* **1**, 2876–2890.
46 Micsonai A, Moussong É, Wien F, Boros E, Vadászi H, Murvai N, Lee Y-H, Molnár T, Réfrégiers M and Goto Y (2022) BeStSel: webserver for secondary structure and fold prediction for protein CD spectroscopy. *Nucleic Acids Res* **50**, W90–W98.
47 Patel K and Golemi-Kotra D (2015) Signaling mechanism by the Staphylococcus aureus two-component system LytSR: role of acetyl phosphate in bypassing the cell membrane electrical potential sensor LytS. *F1000Res* **4**, 79.
48 Cole D, Young G, Weigel A, Sebesta A and Kukura P (2017) Label-free single-molecule imaging with numerical-aperture-shaped interferometric scattering microscopy. *ACS Photonics* **4**, 211–216.
49 Case DA, Aktulga HM, Belfon K, Cerutti DS, Cisneros GA, Cruzeiro VWD, Forouzesh N, Giese TJ and Götz AW & Gohlke, H (2023) AmberTools. *J Chem Inf Model* **63**, 6183–6191.
50 Jo S, Kim T, Iyer VG and Im W (2008) CHARMM-GUI: a web-based graphical user interface for CHARMM. *J Comput Chem* **29**, 1859–1865.
51 Maier JA, Martinez C, Kasavajhala K, Wickstrom L, Hauser KE and Simmerling C (2015) ff14SB: improving the accuracy of protein side chain and backbone parameters from ff99SB. *J Chem Theory Comput* **11**, 3696–3713.
52 Jorgensen WL, Chandrasekhar J, Madura JD, Impey RW and Klein ML (1983) Comparison of simple potential functions for simulating liquid water. *J Chem Phys* **79**, 926–935.
53 Li P, Song LF, and Merz KM Jr (2015) Systematic parameterization of monovalent ions employing the nonbonded model. *J Chem Theory Comput* **11**, 1645–1657.
54 Sengupta A, Li Z, Song LF, Li P, and Merz KM Jr (2021) Parameterization of monovalent ions for the OPC3, OPC, TIP3P-FB, and TIP4P-FB water models. *J Chem Inf Model* **61**, 869–880.
55 Olsson MH, Søndergaard CR, Rostkowski M and Jensen JH (2011) PROPKA3: consistent treatment of internal and surface residues in empirical p K a predictions. *J Chem Theory Comput* **7**, 525–537.
56 Søndergaard CR, Olsson MH, Rostkowski M and Jensen JH (2011) Improved treatment of ligands and coupling effects in empirical calculation and rationalization of p K a values. *J Chem Theory Comput* **7**, 2284–2295.
57 Åqvist J, Wennerström P, Nervall M, Bjelic S and Brandsdal BO (2004) Molecular dynamics simulations of water and biomolecules with a Monte Carlo constant pressure algorithm. *Chem Phys Lett* **384**, 288–294.
58 Ryckaert J-P, Ciccotti G and Berendsen HJ (1977) Numerical integration of the cartesian equations of motion of a system with constraints: molecular dynamics of n-alkanes. *J Comput Phys* **23**, 327–341.
59 Humphrey W, Dalke A and Schulten K (1996) VMD: visual molecular dynamics. *J Mol Graph* **14**, 33–38.
60 Romo TD and Grossfield A (2009) LOOS: an extensible platform for the structural analysis of simulations. In *2009 Annual International Conference of the IEEE Engineering in Medicine and Biology Society*pp. 2332–2335. IEEE,
61 Romo TD, Leioatts N and Grossfield A (2014) Lightweight object oriented structure analysis: tools for building tools to analyze molecular dynamics simulations. *J Comput Chem* **35**, 2305–2318.
62 Michaud-Agrawal N, Denning EJ, Woolf TB and Beckstein O (2011) MDAnalysis: a toolkit for the analysis of molecular dynamics simulations. *J Comput Chem* **32**, 2319–2327.
63 Gowers RJ, Linke M, Barnoud J, Reddy TJE, Melo MN, Seyler SL, Domanski J, Dotson DL, Buchoux S and Kenney IM (2019) *MDAnalysis: A Python Package for the Rapid Analysis of Molecular Dynamics Simulations*. Los Alamos National Laboratory (LANL), Los Alamos, NM (United States).
64 Beutler TC, Mark AE, Van Schaik RC, Gerber PR, Van Gunsteren WF (1994) Avoiding singularities and numerical instabilities in free energy calculations based on molecular simulations. *Chem Phys Lett* **222**, 529–539.
65 Guerois R, Nielsen JE and Serrano L (2002) Predicting changes in the stability of proteins and protein complexes: a study of more than 1000 mutations. *J Mol Biol* **320**, 369–387.
66 Xie O, Chisholm RH, Featherstone L, Nguyen ANT, Hayes AJ, Jespersen MG, Zachreson C, Tellioglu N, Tonkin-Hill G, Dotel R *et al*. (2025) Temporal and

22115463, 0, Downloaded from https://febs.onlinelibrary.wiley.com/doi/10.1002/2211-5463.70275 by University Of Technology Sydney, Wiley Online Library on [08/10/2026]. See the Terms and Conditions (https://onlinelibrary.wiley.com/terms-and-conditions) on Wiley Online Library for rules of use; OA articles are governed by the applicable Creative Commons License

geographical lineage dynamics of invasive streptococcus pyogenes in Australia from 2011 to 2023: a retrospective, multicentre, clinical and genomic epidemiology study. *Lancet Microbe* **6**, 101053.
67 Engleberg NC, Heath A, Miller A, Rivera C and Dirita VJ (2001) Spontaneous mutations in the CsrRS two-component regulatory system of streptococcus pyogenes result in enhanced virulence in a murine model of skin and soft tissue infection. *J Infect Dis* **183**, 1043–1054.
68 Tran-Winkler HJ, Love JF, Gryllos I and Wessels MR (2011) Signal transduction through CsrRS confers an invasive phenotype in group A streptococcus. *PLoS Pathog* **7**, e1002361.
69 Langshaw EL, Reynolds S, Ozberk V, Dooley J, Calcutt A, Zaman M, Walker MJ, Batzloff MR, Davies MR, Good MF *et al.* (2023) Streptolysin O deficiency in streptococcus pyogenes M1T1 covR/S mutant strain attenuates virulence in in vitro and in vivo infection models. *MBio* **14**, e0348822.
70 Lyu PC, Sherman JC, Chen A and Kallenbach NR (1991) Alpha-helix stabilization by natural and unnatural amino acids with alkyl side chains. *Proc Natl Acad Sci USA* **88**, 5317–5320.

Supporting information

Additional supporting information may be found online in the Supporting Information section at the end of the article.

Fig. S1. *In vivo* $M1_{UK}$ subcutaneous infection.
Fig. S2. Recombinant CovR purification and mass photometry standard curve.
Fig. S3. CovR molecular dynamics simulations.
Table S1. Identification of point mutations in $M1_{UK}$ strain SP1448 via whole genome sequencing following animal passage.
Table S2. Relative stability for Ala111Val mutants based on free energy calculations.
Table S3. Summary of molecular dynamics (MD) simulated systems.
Table S4. Summary of free-energy perturbation (FEP) dynamics simulated systems.

FEBS Open Bio (2026) © 2026 The Author(s). *FEBS Open Bio* published by John Wiley & Sons Ltd on behalf of Federation of European Biochemical Societies.

22115463, 0, Downloaded from https://febs.onlinelibrary.wiley.com/doi/10.1002/2211-5463.70275 by University Of Technology Sydney, Wiley Online Library on [08/10/2026]. See the Terms and Conditions (https://onlinelibrary.wiley.com/terms-and-conditions) on Wiley Online Library for rules of use; OA articles are governed by the applicable Creative Commons License